

RESEARCH ARTICLE | MARCH 08 2024

Free-energy landscape and spinodals for the liquid–liquid transition of the TIP4P/2005 and TIP4P/Ice models of water

Special Collection: [Water: Molecular Origins of its Anomalies](#)

Francesco Sciortino  ; Thomas E. Gartner, III ; Pablo G. Debenedetti 

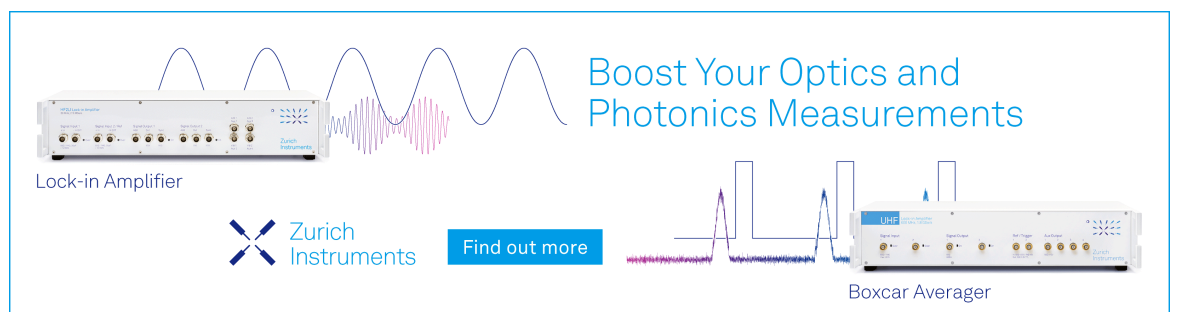
 Check for updates

J. Chem. Phys. 160, 104501 (2024)

<https://doi.org/10.1063/5.0196964>




CrossMark



Boost Your Optics and
Photonics Measurements

Lock-in Amplifier

 Zurich
Instruments

[Find out more](#)

Boxcar Averager

Free-energy landscape and spinodals for the liquid–liquid transition of the TIP4P/2005 and TIP4P/Ice models of water

Cite as: J. Chem. Phys. 160, 104501 (2024); doi: 10.1063/5.0196964

Submitted: 10 January 2024 • Accepted: 20 February 2024 •

Published Online: 8 March 2024



View Online



Export Citation



CrossMark

Francesco Sciortino,^{1,a)}  Thomas E. Gartner III,²  and Pablo G. Debenedetti³ 

AFFILIATIONS

¹ Dipartimento di Fisica, Sapienza Università di Roma, Piazzale Aldo Moro 5, I-00185 Rome, Italy

² Department of Chemical and Biomolecular Engineering, Lehigh University, Bethlehem, Pennsylvania 18015, USA

³ Department of Chemical and Biological Engineering, Princeton University, Princeton, New Jersey 08544, USA

Note: This paper is part of the JCP Special Topic on Water: Molecular Origins of its Anomalies.

^{a)} Author to whom correspondence should be addressed: francesco.sciortino@uniroma1.it

ABSTRACT

Continued increases in computational power now make it possible to evaluate the free-energy landscape associated with the first-order liquid–liquid transition in realistic models of water for which an accurate estimate of the liquid–liquid critical point exists, and to explore its change with pressure near the coexistence line. We report the results of 50 μ s-long NPT umbrella sampling simulations for two realistic models for water, TIP4P/2005 and TIP4P/ice, 3–9 K below their critical temperatures. The free energy profile at different pressures clearly shows the presence of two well-defined free energy basins and makes it possible to identify the liquid–liquid spinodal points, the limits of stability that define the (temperature dependent) pressure range within which two distinct free energy basins exist. The results show that for temperatures less than 10 K below the critical temperature, metastable states are possible across a very limited pressure interval, information that is relevant to the interpretation of experiments probing the metastable phase behavior of deeply supercooled water in the so-called no-man’s land.

Published under an exclusive license by AIP Publishing. <https://doi.org/10.1063/5.0196964>

I. INTRODUCTION

From a computational perspective, there is now overwhelming evidence that supercooled water undergoes a liquid–liquid transition at sufficiently low temperatures and positive pressures. Beginning with the initial observation in 1992 by Poole, Sciortino, Essmann, and Stanley,¹ critical fluctuations have been reported for several classical rigid-water molecular models,^{2–7} monoatomic models,⁸ flexible and polarizable models,⁹ as well as machine-learned force fields trained on *ab initio* data, such as density functional theory (DFT).^{10,11} Near the critical point, constant pressure simulations display significant volume fluctuations,^{4,7} indicating the preferential exploration of two local structures with similar free energies but different densities, the prodrome of low- and high-density liquids (LDL and HDL). The analysis of these fluctuations revealed a precise correspondence with the magnetization fluctua-

tions in the three-dimensional Ising model,¹² confirming the existence of a critical point in the 3D scalar order parameter universality class.

Simulations in the region of the liquid–liquid critical point are quite demanding. Relaxation times are of the order of μ s (even more for densities smaller than 1 g/cm³), and a large effort is required simply to equilibrate the studied system, before starting the acquisition of statistically meaningful data. This computational difficulty has prevented accurate computational studies of water below the critical temperature. In this article, we report 40 μ s (or more) molecular dynamics (MD) simulations for two of the best rigid water models, TIP4P/2005¹³ and TIP4P/Ice water,¹⁴ a few degrees below the liquid–liquid critical temperature to quantify the free energy profile. We clearly detect the presence of two distinct minima, separated by a barrier. We also investigate how the profile changes with pressure to identify the location of the limit of stability of the two liquids

(the spinodal pressures). This information is relevant to the interpretation of recent outstanding experiments¹⁵ that have started to approach the critical point region in no-man's land. We find, as expected when the temperature is not much smaller than the critical temperature T_c , that the barrier is a few $k_B T$ and that the range of pressures where a metastable liquid basin can exist is only few hundred bar.

II. METHODS

A. Umbrella sampling simulations

Molecular dynamics simulations of a system of $N = 1000$ TIP4P/2005 or TIP4P/Ice¹⁴ water molecules were performed in the NPT ensemble using GROMACS 2021.4^{16,17} in single precision patched with PLUMED¹⁸ (plumed-2.8.1). The integration of the equations of motion was performed with a leapfrog integrator with a 2 fs time step, temperature coupling was controlled using a Bussi thermostat (v-rescale)¹⁹ with a characteristic time of 4 ps, and pressure coupling was controlled using an isotropic Parrinello–Rahman barostat²⁰ with a characteristic time of 12 ps. The molecular constraints were implemented by a sixth-order linear constraint solver (LINCS) algorithm.²¹ A cutoff distance of 0.9 nm was selected for van der Waals forces, and electrostatic interactions were evaluated with a fourth-order particle-mesh Ewald method,²² with a real-space cutoff of 0.9 nm. A harmonic umbrella sampling (US) potential,^{23,24}

$$W_{\text{US}} = \frac{1}{2}K(V - V_0)^2, \quad (1)$$

was added (via PLUMED) to the Hamiltonian to force the system to explore volumes (V) close to the setpoint volume V_0 . Sixteen different values of V_0 were investigated, covering the range $26.7 < V_0 < 32.4 \text{ nm}^3$ (corresponding approximately to densities between 0.95 and 1.1 g/cm^3). The selected P and T for the US simulations were $P_{\text{sim}} = 1900 \text{ bars}$ and $T_{\text{sim}} = 180 \text{ K}$ for TIP4P/Ice (for which $T_c = 188.6 \pm 1 \text{ K}$ and $P_c = 1746 \pm 6 \text{ bars}$ when $N = 1000^7$) and $P_{\text{sim}} = 1875 \text{ bars}$ and $T_{\text{sim}} = 170 \text{ K}$ for TIP4P/2005 (for which $T_c = 173.1 \pm 1 \text{ K}$ and $P_c = 1850 \pm 9 \text{ bars}$ when $N = 1000^7$). The elastic constant K in Eq. (1) was fixed at $20 \text{ kJ mol}^{-1} \text{ nm}^{-6}$ in the case of TIP4P/Ice and $30 \text{ kJ mol}^{-1} \text{ nm}^{-6}$ in the case of TIP4P/2005.

For each V_0 , simulations of length $75 \mu\text{s}$ (TIP4P/Ice) or $50 \mu\text{s}$ (TIP4P/2005) were performed, of which the first third were considered as an equilibration period and excluded from all subsequent analysis. Each simulation was run on eight cores (10^8 steps/day), resulting approximately in $1 \mu\text{s}$ every five days, for a total of 260 cores running full time for eight months. The starting configurations (each of them with $V \approx V_0$) were selected from Ref. 25. These configurations had been equilibrated for several tens of μs at $T = 188 \text{ K}$ with the TIP4P/Ice model and used as starting configurations for the present runs. To highlight the difficulty in equilibrating the LDL at these low temperatures, we show in Fig. 1 the evolution of the volume in one of the US simulations for a value of V_0 corresponding to the low density liquid in two different runs, starting in one case at a volume close to V_0 and in the other at a different volume. Only after $30 \mu\text{s}$ do the two systems converge to the same (equilibrium) volume. The difficulty of equilibration even at $T_{\text{sim}} = 180 \text{ K}$ is the reason why we chose a different distance from the critical point

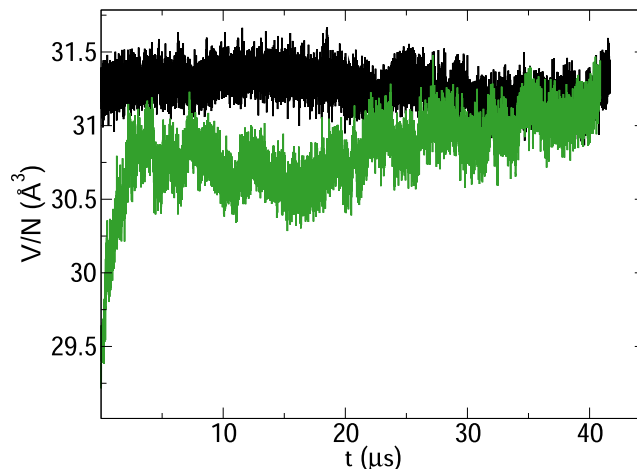


FIG. 1. Evolution of the volume per particle (V/N) during US simulations of $N = 1000$ molecules with $V_0 = 31.2 \text{ nm}^3$ for the TIP4P/Ice model ($P_{\text{sim}} = 1900 \text{ bars}$ and $T_{\text{sim}} = 180 \text{ K}$). The two curves correspond to two different initial volumes, one close to V_0 (black) and one smaller (green).

($T_c - T_{\text{sim}}$) between the TIP4P/2005 and TIP4P/Ice models. If we wanted to simulate at the same distance from the critical point for both models, we would need to choose $T_{\text{sim}} \approx 164 \text{ K}$ for TIP4P/2005, which is essentially impossible to equilibrate with current computational resources due to the proximity of that model's glass transition temperature.²⁶

We also performed a limited number of standard NPT MD simulations at T_{sim} and different pressures, starting from both low- and high-density configurations (selected from Ref. 25). These standard simulations, of which some are longer than $100 \mu\text{s}$, make it possible to follow the unbiased evolution of the density and the presence of metastability.

B. Analysis

The output of each NPT US simulation is the time series of the system volume. From this time series, the distribution of sampled volumes $\mathcal{P}_{V_0}(V)$ can be directly calculated. Apart from a normalization constant, the distribution provides (over the sampled interval of volumes) a measure of the *restricted* Gibbs free energy G at the selected P_{sim} and T_{sim} , since (indicating with the symbol X_{V_0} that the function X refers to the simulation at fixed V_0 and with β the inverse of the thermal energy $k_B T$)

$$\mathcal{P}_{V_0}(V) \sim e^{-\beta[G_{V_0}(V) + W_{\text{US}}(V, V_0)]}, \quad (2)$$

$$\beta G_{V_0}(V) = -\ln \mathcal{P}_{V_0}(V) - \frac{1}{2}\beta K(V - V_0)^2 + \text{constant}. \quad (3)$$

Splicing together $\beta G_{V_0}(V)$ calculated from different V_0 windows by adding to each window an appropriate constant, it becomes possible to reconstruct the entire $\beta G(V)$ profile.

A more sophisticated approach to evaluating $\beta G(V)$, which we also used in this work, based on the simultaneous minimization of the statistical error over all explored V_0 windows is provided by the so-called weighted histogram analysis method

(WHAM).²⁷ Code implementing this method is available open access.²⁸

A further independent estimate of $\beta G(V)$ can be derived by exploiting the relation between the free energy in the presence and the free energy in the absence of the umbrella potential,²⁹

$$\beta G_{\text{US}}(V) = \beta G(V) + \frac{1}{2}\beta K(V - V_0)^2. \quad (4)$$

Expanding up to the first order $\beta G(V)$ around V_0 , one obtains

$$\beta G_{\text{US}}(V) = \beta G(V_0) + \frac{d\beta G}{dV}\bigg|_{V_0} (V - V_0) + \frac{1}{2}\beta K(V - V_0)^2. \quad (5)$$

The most probable volume in the US simulation is the one that minimizes $\beta G_{\text{US}}(V)$. By equating to zero the derivative of Eq. (5), one finds

$$\frac{d\beta G(V)}{dV}\bigg|_{V_0} = -\beta K(\langle V \rangle_{V_0} - V_0), \quad (6)$$

where we have identified the minimum V_{min} of $\beta G_{\text{US}}(V)$ with the average volume sampled in the US simulation $\langle V \rangle_{V_0}$.

Then, simply by evaluating in each window $\langle V \rangle_{V_0} - V_0$, one obtains information on the volume derivative of the (unbiased) free energy. An integration over the volume of $\frac{d\beta G(V)}{dV}\bigg|_{V_0}$ provides an independent estimate of the V dependence of $\beta G(V)$ (apart from an integration constant).

Once the volume dependence of the Gibbs free energy has been calculated at T_{sim} and P_{sim} of the simulation, it is possible to predict the same function for different values of the pressure (since the Helmholtz free energy does not depend on pressure explicitly),

$$\beta G(T_{\text{sim}}, P, V) = \beta G(T_{\text{sim}}, P_{\text{sim}}, V) - \beta(P_{\text{sim}} - P)V. \quad (7)$$

III. RESULTS

A. TIP4P/Ice

Estimates of the location of the critical point for the TIP4P/Ice model include Ref. 7 ($T_c = 188.6 \pm 1$ K and $P_c = 1746 \pm 6$ bars; comparison of density fluctuations with the 3D Ising model), Ref. 30 ($T_c = 188$ –203 K and $P_c = 1500$ –1650 bars; analysis of the magnitude of maxima along the locus of maximum compressibility), and Ref. 31 ($T_c = 195 \pm 5$ K and $P_c = 1650 \pm 150$ bars; intersection of extrapolated loci of heat capacity and compressibility maxima). In this work, we choose to use as a reference the above-cited critical point for a 1000 molecule system obtained in Ref. 7, given the high-precision estimate of the critical parameters afforded by comparing near-critical density fluctuations to the 3D Ising model. In the NPT simulations, we fix $T_{\text{sim}} = 180$ K and $P_{\text{sim}} = 1900$ bars.

Figure 2(a) shows $\beta G_{V_0}(V)$ [see Eq. (3)] for all investigated V_0 windows to share the raw data of this investigation. By comparing two adjacent windows, for each set of data, the best shift constant can be identified (for example with least-square fit of the difference of all overlapping points) to reconstruct the volume dependence of the Gibbs free energy. The result of this operation is shown in Fig. 3, together with the optimized simultaneous fit over all data provided by WHAM.

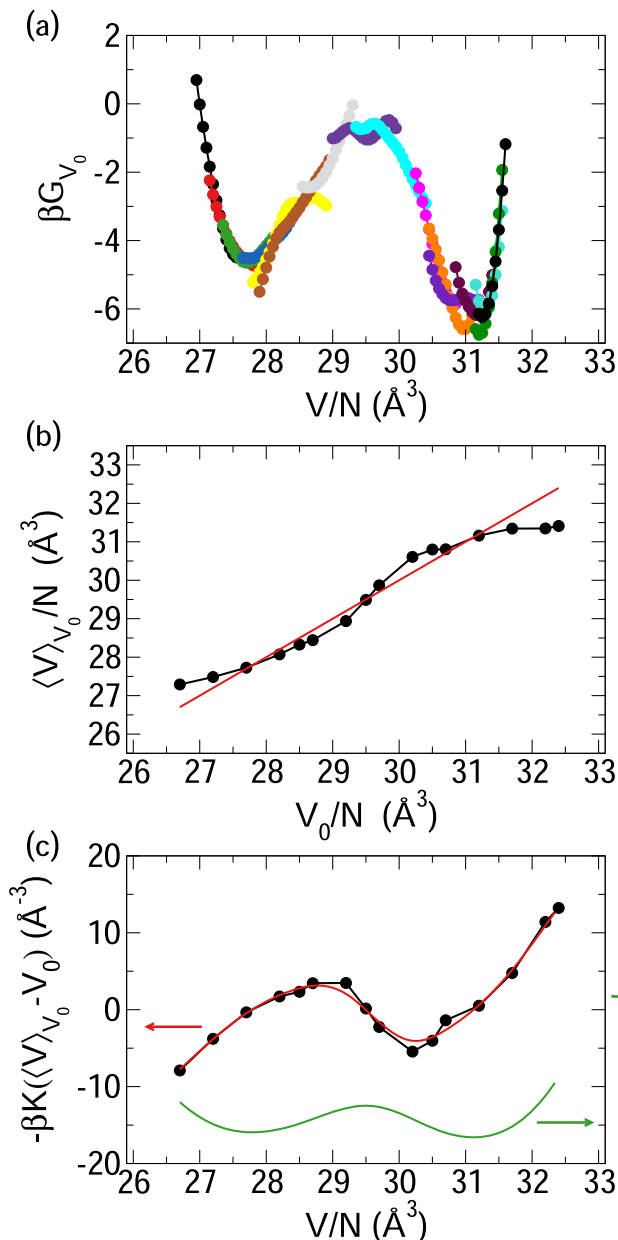


FIG. 2. Raw US data for TIP4P/Ice. (a) βG_{V_0} for all investigated US windows. Data have been shifted to minimize the difference in the free-energy estimate between adjacent windows in the common range of volumes. Each window is plotted in a different color. (b) Plot of $\langle V \rangle_{V_0}$ vs V_0 (black), with the line $\langle V \rangle_{V_0} = V_0$ in red. (c) Plot of $-\beta K(\langle V \rangle_{V_0} - V_0)$ vs V_0 (points, left axis), a seventh-order polynomial fit (red curve, left axis), and the integral of the polynomial fit to obtain the free energy (green curve, right axis). The left and right y-axes have the same numerical scale: the distance between major ticks is 10.

Figure 2(b) shows the average volume $\langle V \rangle_{V_0}$ as a function of V_0 . Figure 2(c) shows the right side of Eq. (6), the volume derivative of βG . A spline function through the data provides a convenient numerical expression for rebuilding, by integration,

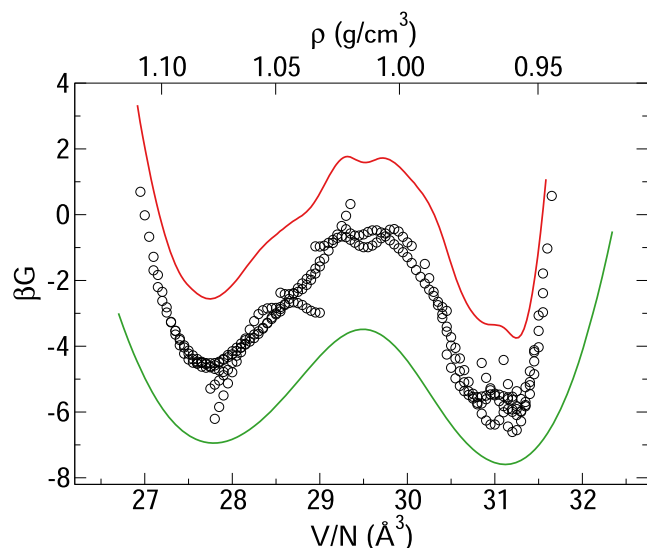


FIG. 3. Different numerical estimates of $\beta G(V)$ for TIP4P/Ice ($N = 1000$, $T_{sim} = 180$ K, $P_{sim} = 1900$ bars). Three different methods are compared: (i) best overlap between adjacent windows (black circles), (ii) WHAM estimate (red curve), and (iii) evaluation of the free energy slope via $\langle V \rangle_{V_0} - V_0$ (green curve). The curves have been shifted vertically for clarity. The mass density (ρ) is included as an alternate x axis.

the volume dependence of βG . The result is also reported in Fig. 3.

All three methods yield a Gibbs free energy consistent with a free energy barrier of $3\text{--}4 k_B T$, separating two basins, centered around volume per molecule of 28 and 32 \AA^3 (corresponding to the densities of 1.068 and 0.934 g/cm^3 , respectively). Of course, the barrier heights would increase away from the critical temperature (lower T), but it then becomes even more challenging to properly equilibrate the system.

Finally, Fig. 4 shows βG reweighted to different values of P , calculated according to Eq. (7). The typical scenario characteristic of first order transitions appears. At pressures below $P \approx 1800$ bars, a single (low-density liquid) minimum is observed. Similarly, for pressures above $P \approx 2000$ bars, only the high-density liquid minimum exists. In the intermediate pressure range ($1800 \leq P \leq 2000$ bars), the Gibbs free energy shows two distinct minima, whose relative free energy varies continuously with P . This interval brackets the two spinodal points associated with the liquid–liquid first-order transition. We note in passing that, while the barrier is clearly present, its height is within a few $k_B T$, suggesting that, at this temperature (and this system size), thermal fluctuations can cause the liquid to fluctuate between the two phases, even at or close to the coexistence pressure. The data in Fig. 4 also imply that no simulation started from an equilibrated HDL configuration brought to a pressure smaller than 1800 bars can remain in a metastable HDL state at this temperature. The density in the MD run will evolve continuously toward the LDL basin. Similarly, any simulations equilibrated in the LDL basin and pressurized above 2000 bars will continuously evolve to the high density phase.

To confirm the previous results with independent calculations, Fig. 5 shows the time dependence of the volume as a function of

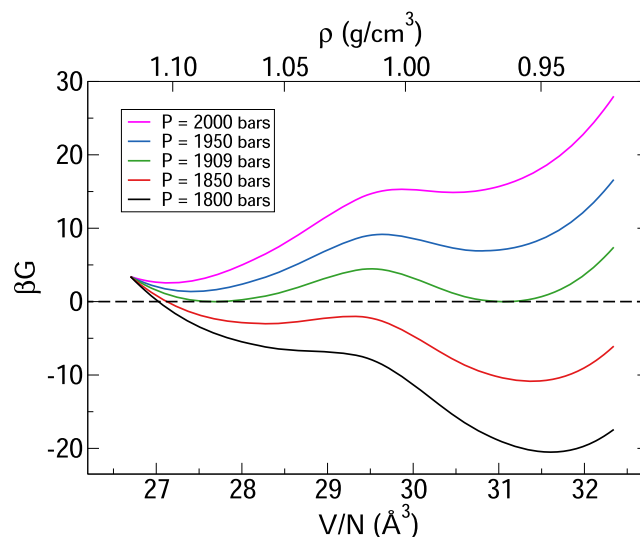


FIG. 4. Gibbs free energies [Eqs. (6) and (7)] reweighted to different pressures as marked, as a function of the volume per particle for TIP4P/Ice at $T_{sim} = 180$ K. The curves have been shifted to coincide at the lowest studied volume. The mass density (ρ) is included as an alternate x axis.

time, at $P_{sim} = 1900$ bars and below in a standard NPT simulation (at $T_{sim} = 180$ K). While at $P_{sim} = 1900$ bars, simulations starting from low- and high-density configurations remain in equilibrium in their own free-energy basin for more than 120 μs , the simulations at lower pressures, independent of their starting density, evolve toward the

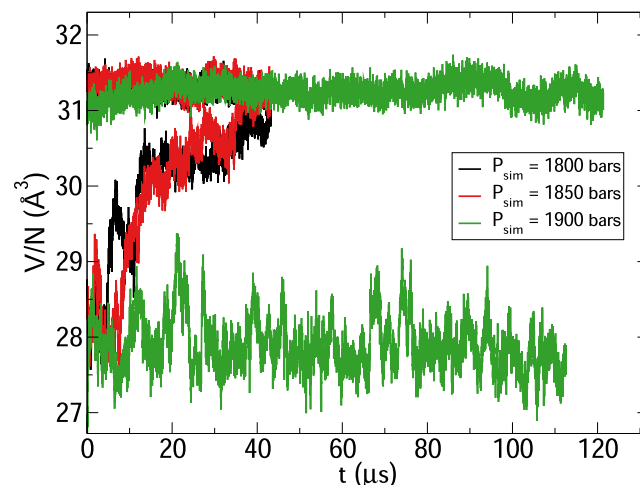


FIG. 5. Unbiased NPT MD simulations at $T_{sim} = 180$ K for TIP4P/Ice. Black is $P_{sim} = 1800$ bars, red is $P_{sim} = 1850$ bars, and green is $P_{sim} = 1900$ bars. For each pressure, simulations are started from configurations in the LDL and HDL phases. Note that when P_{sim} is close to the coexistence pressure (1900 bars), for more than 120 μs , no transition between the two basins is observed. Differently, for pressures lower than coexistence, the simulations starting from the HDL phase convert (but after several μs) to the LDL phase.

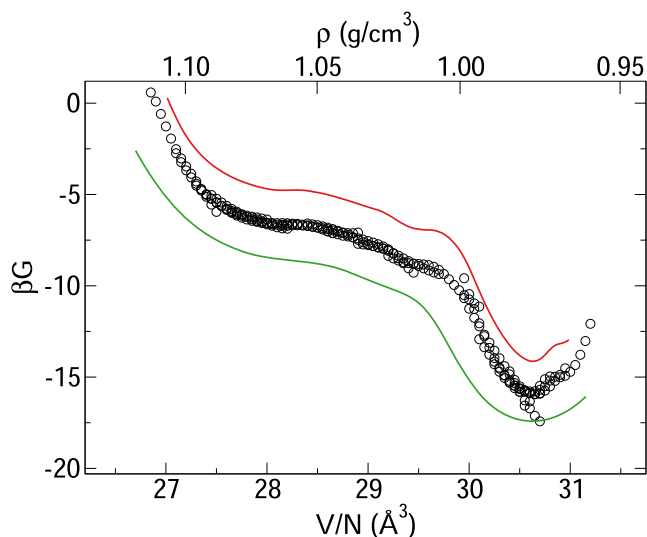


FIG. 6. Different numerical estimates of $\beta G(V)$ for the TIP4P/2005 model ($N = 1000$, $T_{sim} = 170$ K, $P_{sim} = 1875$ bars). Three different methods are compared: (i) best overlap between adjacent windows (black circles), (ii) WHAM estimate (red curve), and (iii) evaluation of the free energy slope via $\langle V \rangle_{V_0} - V_0$ (green curve). The curves have been shifted vertically for clarity. The mass density (ρ) is included as an alternate x axis.

large volume (low density) phase. The two average volumes coincide with the position of the two minima of $\beta G(V)$ (see Fig. 3).

B. TIP4P/2005

There are several estimates for the critical parameters of TIP4P/2005, including via numerical analysis of the equation of state

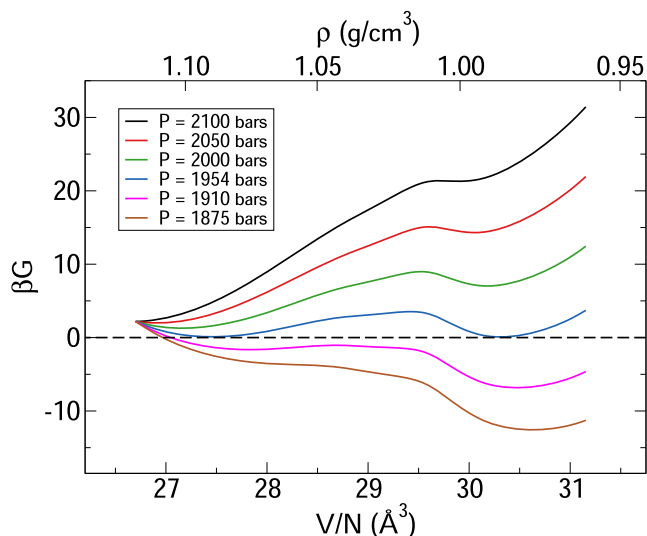


FIG. 7. Gibbs free energies [Eqs. (6) and (7)] for the TIP4P/2005 model reweighted to different pressures as marked, as a function of the volume per particle at $T_{sim} = 170$ K. The curves have been shifted to coincide at the lowest studied volume. The mass density (ρ) is included as an alternate x axis.

in the near-critical region, yielding $T_c = 193$ K and $P_c = 1350$ bars,³² two-state model fits to the energy landscape, yielding $T_c = 175 \pm 2$ K and $P_c = 1750 \pm 20$ bars,³³ or two-state model fits to the equation of state data, yielding $T_c = 182$ K and $P_c = 1700$ bars.³⁴ As above, we take as the critical point the high-precision estimate obtained for a 1000 molecule TIP4P/2005 system in comparison with the Ising model, $T_c = 173.1 \pm 1$ K and $P_c = 1850 \pm 9$ bars.⁷ In the NPT simulations, we fix $T_{sim} = 170$ K and $P_{sim} = 1875$ bars. The critical point of TIP4P/2005 is about 16 K lower than the one of TIP4P/Ice, which makes it even more challenging to properly equilibrate the studied samples.

Figure 6 shows the Gibbs free energy calculated with the three distinct methods. The three very similar estimates suggest that P_{sim} is in the region where the low-density liquid is stable, suggesting that,

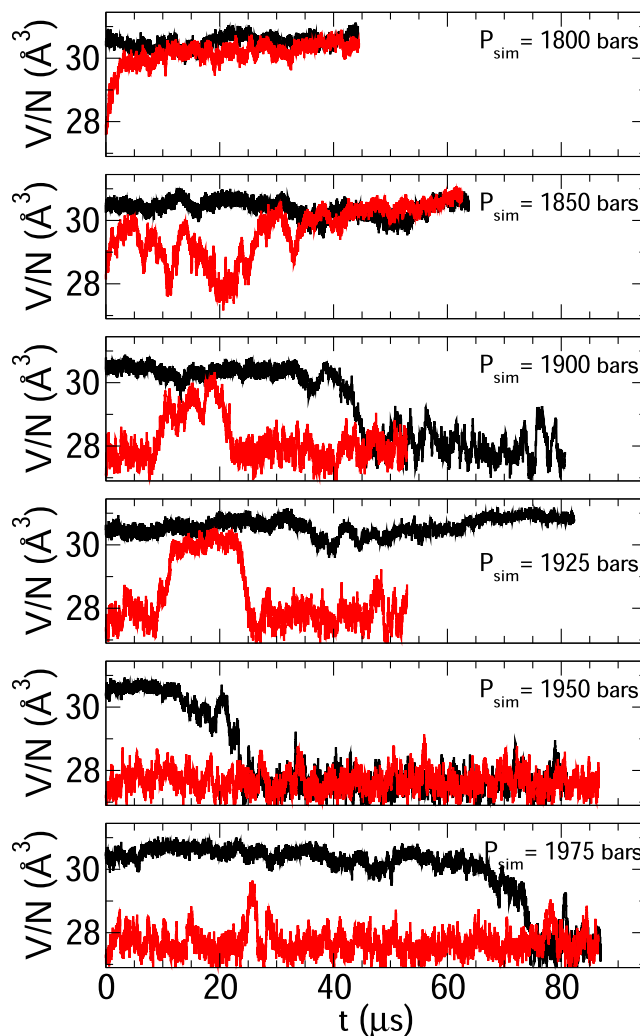


FIG. 8. Unbiased NPT MD simulations for six different pressures at $T_{sim} = 170$ K for TIP4P/2005 ($N = 1000$). From top to bottom $P_{sim} = 1800, 1850, 1900, 1925, 1950, 1975$ bars. In each panel, two different runs are shown, both at the same pressure but one starting from an HDL (red curve) configuration and the other starting from an LDL (black curve) configuration.

at this pressure, any simulation starting from the HDL phase should continuously transform into LDL.

To estimate the coexistence pressure and the spinodal points, we calculate βG reweighted to different values of P , according to Eq. (7). The resulting free energy profiles are shown in Fig. 7. This figure shows that the model's coexistence pressure is 1954 bars, and the low and high pressure spinodal points are approximately at 1875 and 2100 bars, respectively. As for TIP4P/Ice, the barrier at coexistence is $\sim 3 k_B T$ for this system size. Because T_{sim} for the TIP4P/2005 simulations is slightly less subcritical than T_{sim} for TIP4P/Ice, we would expect the width of the spinodal and the height of the barrier in our calculations to be slightly smaller for TIP4P/2005. The data appear consistent with this expectation, although the trends are slight.

As done for the TIP4P/Ice model, we also confirm with independent calculations the above results for the TIP4P/2005 model. Figure 8 shows the time dependence of the volume for different pressures for times up to 80 μs in standard NPT simulations. In the top panel, both simulations converge to LDL; in the central ones, a more erratic behavior is observed (with a significant metastability); and in the lower panels (for $P_{sim} = 1950$ and 1975 bars), both simulations converge at very long time to HDL values.

IV. CONCLUSIONS

The liquid–liquid critical point hypothesis, proposed in 1992 to explain the anomalous thermodynamic behavior of water,¹ particularly in supercooled states, has recently received computational confirmation in several water models, including those incorporating polarizable⁹ and DFT-based neural network potentials.¹¹ Notably, the TIP4P/2005 and TIP4P/Ice models^{13,14} offer a significant platform for investigating the physics in close proximity to the liquid–liquid critical point, due to their useful combination of computational efficiency and accuracy relative to available experimental data.

Indeed, with modern computational resources, it is now feasible to equilibrate systems of water molecules within the temperature–pressure range where the critical point is situated. In this study, prompted, in part, by a recent numerical investigation disputing the existence of free-energy barriers in the TIP4P/2005 landscape,³⁵ we have focused on the thermodynamic behavior ~ 3 – 9 K below the critical point. Our aim is to unequivocally demonstrate the presence of a free-energy barrier that separates the two liquid phases and to estimate the pressure range encompassing the two spinodal points, which represent the mean-field limit of stability for the low-density liquid (LDL) and high-density liquid (HDL) phases.

Our extensive computational study has unveiled a discernible barrier of 3 – $4 k_B T$, effectively separating the two liquid phases. The temperatures and pressures at which we observe coexistence are consistent with the critical point locations identified in Ref. 7. At reduced temperatures of ~ 0.96 , we have also characterized and found the region of metastability for the LDL and HDL phases to be rather restricted in terms of pressure, spanning ~ 200 bars. The low height of the free energy barrier and the limited region of metastability suggest that even when operating 10 K below the critical point, precise control of external pressure is required to observe coexistence between the two liquid phases. These findings align with

recent experimental results in which the transition between HDL and LDL showed no discernible nucleation time.¹⁵

We emphasize that the limited pressure range of the spinodal interval elucidates one possible source of the erroneous conclusions presented in Ref. 35, where the chosen pressure (very close to the spinodal limit) prevented the observation of the free energy barrier and of the underlying physics of liquid–liquid coexistence. We also note that, in the current work, unbiased simulations within the metastable regime show a stochastic behavior, with transitions between basins occurring over a broad range of timescales. Our results underscore the need for careful free energy calculations to evaluate the liquid–liquid phase behavior and that further work is needed to comprehensively explore the kinetics of the transition.

SUPPLEMENTARY MATERIAL

The supplementary material presents a study of the convergence of the numerical results as a function of the total simulation time.

ACKNOWLEDGMENTS

F.S. acknowledges the support from MIUR-PRIN Grant No. 2022JWAF7Y, Cineca ISCRA initiative, and ICSC-Centro Nazionale di Ricerca in High Performance Computing, Big Data and Quantum Computing, funded by the European Union (“NextGenerationEU”).

AUTHOR DECLARATIONS

Conflict of Interest

The authors have no conflicts to disclose.

Author Contributions

Francesco Sciortino: Conceptualization (equal); Data curation (lead); Writing – original draft (lead); Writing – review & editing (equal). **Thomas E. Gartner III:** Conceptualization (equal); Writing – review & editing (equal). **Pablo G. Debenedetti:** Conceptualization (equal); Writing – review & editing (equal).

DATA AVAILABILITY

The data that support the findings of this study are available within the article. The GROMACS, PLUMED, and WHAM codes are available at Refs. 16–18 and 28. Additional data (trajectories) are available from the corresponding author upon reasonable request.

REFERENCES

- 1 P. H. Poole, F. Sciortino, U. Essmann, and H. E. Stanley, *Nature* **360**, 324 (1992).
- 2 Y. Liu, A. Z. Panagiotopoulos, and P. G. Debenedetti, *J. Chem. Phys.* **131**, 104508 (2009).
- 3 F. Sciortino, I. Saika-Voivod, and P. H. Poole, *Phys. Chem. Chem. Phys.* **13**, 19759 (2011).
- 4 T. A. Kesselring, G. Franzese, S. V. Buldyrev, H. J. Herrmann, and H. E. Stanley, *Sci. Rep.* **2**, 474 (2012).
- 5 J. C. Palmer, F. Martelli, Y. Liu, R. Car, A. Z. Panagiotopoulos, and P. G. Debenedetti, *Nature* **510**, 385 (2014).
- 6 J. C. Palmer, P. H. Poole, F. Sciortino, and P. G. Debenedetti, *Chem. Rev.* **118**, 9129 (2018).

- ⁷P. G. Debenedetti, F. Sciortino, and G. H. Zerze, *Science* **369**, 289 (2020).
- ⁸D. Dhabal, R. Kumar, and V. Molinero, "Liquid-liquid transition in a machine-learned coarse grained water model," *chemRxiv* (2023).
- ⁹J. Weis, F. Sciortino, A. Z. Panagiotopoulos, and P. G. Debenedetti, *J. Chem. Phys.* **157**, 024502 (2022).
- ¹⁰T. E. Gartner III, L. Zhang, P. M. Piaggi, R. Car, A. Z. Panagiotopoulos, and P. G. Debenedetti, *Proc. Natl. Acad. Sci. U. S. A.* **117**, 26040 (2020).
- ¹¹T. E. Gartner III, P. M. Piaggi, R. Car, A. Z. Panagiotopoulos, and P. G. Debenedetti, *Phys. Rev. Lett.* **129**, 255702 (2022).
- ¹²N. B. Wilding, *J. Phys.: Condens. Matter* **9**, 585 (1997).
- ¹³J. L. F. Abascal and C. Vega, *J. Chem. Phys.* **123**, 234505 (2005).
- ¹⁴C. Vega, E. Sanz, and J. L. F. Abascal, *J. Chem. Phys.* **122**, 234511 (2005).
- ¹⁵K. H. Kim, K. Amann-Winkel, N. Giovambattista, A. Späh, F. Perakis, H. Pathak, M. L. Parada, C. Yang, D. Mariedahl, T. Eklund, T. J. Lane, S. You, S. Jeong, M. Weston, J. H. Lee, I. Eom, M. Kim, J. Park, S. H. Chun, P. H. Poole, and A. Nilsson, *Science* **370**, 978 (2020).
- ¹⁶D. Van Der Spoel, E. Lindahl, B. Hess, G. Groenhof, A. E. Mark, and H. J. C. Berendsen, *J. Comput. Chem.* **26**, 1701 (2005).
- ¹⁷M. J. Abraham, T. Murtola, R. Schulz, S. Páll, J. C. Smith, B. Hess, and E. Lindahl, *SoftwareX* **1–2**, 19 (2015).
- ¹⁸M. Bonomi, G. Bussi, C. Camilloni, G. A. Tribello, P. Banáš, A. Barducci, M. Bernetti, P. G. Bolhuis, S. Bottaro, D. Branduardi *et al.*, *Nat. Methods* **16**, 670 (2019).
- ¹⁹G. Bussi, D. Donadio, and M. Parrinello, *J. Chem. Phys.* **126**, 014101 (2007).
- ²⁰M. Parrinello and A. Rahman, *J. Appl. Phys.* **52**, 7182 (1981).
- ²¹B. Hess, H. Bekker, H. J. C. Berendsen, and J. G. E. M. Fraaije, *J. Comput. Chem.* **18**, 1463 (1997).
- ²²M. P. Allen and D. J. Tildesley, *Computer Simulation of Liquids*, 2nd ed. (Oxford University Press, Oxford, 2017).
- ²³G. M. Torrie and J. P. Valleau, *J. Comput. Phys.* **23**, 187 (1977).
- ²⁴D. Frenkel and B. Smit, *Understanding Molecular Simulation: From Algorithms to Applications* (Elsevier, 2023).
- ²⁵R. Foffi, J. Russo, and F. Sciortino, *J. Chem. Phys.* **154**, 184506 (2021).
- ²⁶T. E. Gartner III, S. Torquato, R. Car, and P. G. Debenedetti, *Nat. Commun.* **12**, 3398 (2021).
- ²⁷S. Kumar, J. M. Rosenberg, D. Bouzida, R. H. Swendsen, and P. A. Kollman, *J. Comput. Chem.* **13**, 1011 (1992).
- ²⁸See http://membrane.urmc.rochester.edu/wordpress/?page_id=126 for A. Grossfield, "WHAM: The weighted histogram analysis method, version 2.0.11."
- ²⁹U. R. Pedersen, F. Hummel, G. Kresse, G. Kahl, and C. Dellago, *Phys. Rev. B* **88**, 094101 (2013).
- ³⁰J. Škvára and I. Nezbeda, *J. Mol. Liq.* **367**, 120508 (2022).
- ³¹J. R. Espinosa, J. L. F. Abascal, L. F. Sedano, E. Sanz, and C. Vega, *J. Chem. Phys.* **158**, 204505 (2023).
- ³²J. L. F. Abascal and C. Vega, *J. Chem. Phys.* **133**, 234502 (2010).
- ³³P. H. Handle and F. Sciortino, *J. Chem. Phys.* **148**, 134505 (2018).
- ³⁴R. S. Singh, J. W. Biddle, P. G. Debenedetti, and M. A. Anisimov, *J. Chem. Phys.* **144**, 144504 (2016).
- ³⁵A. Jedrecy, A. M. Saitta, and F. Pietrucci, *J. Chem. Phys.* **158**, 014502 (2023).